Power Electronic Systems
Laboratory

Electrical Engineering - Archiv für Elektrotechnik, Springer Link (http://link.springer.com/article/10.1007/s00202-016-0461-7), October 2016

Electromagnetic Field Patterns and Energy Flux of Efficiency Optimal Inductive Power Transfer Systems

R. Bosshard,
T. Guillod,
J. W. Kolar

Eidgenössische Technische Hochschule Zürich
Swiss Federal Institute of Technology Zurich

The final publication is available at http://link.springer.com
DOI: 10.1007/s00202-016-0461-7

Electromagnetic Field Patterns and Energy Flux of Efficiency Optimal Inductive Power Transfer Systems

Roman Bosshard · Thomas Guillod · Johann W. Kolar

Abstract The design of contactless power supplies with Inductive Power Transfer (IPT) is still a challenge even though such systems have become more and more established for various applications. This article presents an intuitive, educational introduction to IPT system design for practicing engineers who are new to the field. While following the path of the energy through the IPT system, the contactless power transfer is explained with a circuit-oriented approach, extended by an analysis of the field patterns and the energy flux across the air gap. Finite element method simulation results for the Poynting vector are shown to illustrate the power transfer process. Finally, a minimization of the reactive power demand of the IPT coils is performed, from which the general requirements for an efficiency optimal design of the IPT system can be intuitively understood.

Keywords Inductive Power Transfer · Electromagnetic Field Theory · Power Electronics · Transformer Design

List of Symbols

L_1	Self-inductance of transmitter coil
L_2	Self-inductance of receiver coil
M	Mutual inductance of the IPT coils
k	Magnetic coupling of the IPT coils
C_1	Transmitter-side compensation capacitance
C_2	Receiver-side compensation capacitance
ω_0	Resonant frequency
$U_{1,\mathrm{DC}}$	Transmitter-side DC input voltage
$U_{2,\mathrm{DC}}$	Receiver-side DC output voltage
P_2	Average output power
$R_{\mathrm{L,eq}}$	Equivalent load resistance
i_1	Transmitter coil current
i_2	Receiver coil current
u_1	Source voltage at transmitter
u_2	Load voltage at receiver
p_{L1}	Input power to IPT coils
p_{L2}	Output power of IPT coils
q_{L1}	Reactive part of input power
q_{L2}	Reactive part of output power
$\mathbf{E}$	Electric field
$\mathbf{H}$	Magnetic field
$\mathbf{S}$	Poynting vector
ϕ	Electric potential
$\mathbf{A}$	Magnetic vector potential
μ_0	Vacuum permeability
ε_0	Vacuum permittivity
w_{m}	Magnetic energy density
w_{e}	Electric energy density
w_{tot}	Total energy density
W_{m}	Total magnetic energy
W_{tot}	Total energy

R. Bosshard (bosshard@lem.ee.ethz.ch)
T. Guillod (guillod@lem.ee.ethz.ch)
Johann W. Kolar (kolar@lem.ee.ethz.ch)

Power Electronic Systems Laboratory
ETH Zurich
Physikstrasse 3
8092 Zurich, Switzerland

1 Introduction

Contactless power supplies using Inductive Power Transfer (IPT) have been proposed for applications ranging from biomedical implants [1, 14, 15], to battery charging systems for portable electronic devices [10, 11, 17] or electric vehicles [2,5–7,9]. Despite the similarity to a conventional power transformer, the characteristics of an IPT system are dominated by the properties of the employed high-order resonant

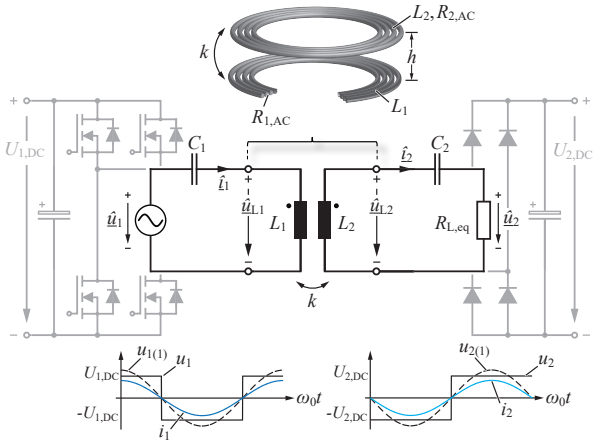

Fig. 1 Fundamental frequency model: the transmitter-side full-bridge inverter is replaced by a sinusoidal voltage source $\hat{\underline{u}}_1$. The receiver-side rectifier is replaced by the equivalent load resistor $R_{L,eq}$ as in [16].

circuits, for which comprehensive expertise is hard to obtain. Therefore, IPT system design remains challenging even though the topic has been studied for several decades. In order to improve the understanding of practicing engineers who are new to the field, this article presents an intuitive, educational approach to the design of IPT systems. Since the purpose of this article is educational, the focus is set on a theoretical analysis of the underlying physical principles and not on a specific application.

By following the path of the energy through the resonant circuit and across the air gap, a natural understanding of the involved physical mechanisms is obtained. The contactless power transfer across the air gap is first explained with the lumped quantities voltage and current, and with the equivalent circuit model of Fig. 1. In Section 2, it is shown that in an IPT system the transferred energy is periodically stored in and extracted from the IPT coil inductances on purpose. This is one of the key differences compared to a conventional transformer. For this reason, the IPT coils are not referred to as a transformer in this work, even though the presented observations apply similarly for a non-ideal transformer with a magnetic coupling close to one.

The equivalent circuit alone is not sufficient for a fundamental understanding of the energy flux through the system. Therefore, in Section 3, the analysis is extended with known concepts from electromagnetic field theory. The periodic energy exchange between the transmitter and the receiver is analyzed more closely on the level of magnetic and electric fields and the energy flux across the air gap is described using Poynting's theorem [4, 8, 12, 13]. From the discussion, the requirements for an efficiency optimal design of the IPT system follow seamlessly and can be intuitively understood. In Section 4, it is demonstrated that the approach pursued in this article coincides with the requirements for an efficiency optimal design of the IPT system that are commonly used in the relevant literature [2, 14, 15, 17]. Finally, in Section 5, a summary of the obtained results and concluding remarks regarding the applicability of the presented theory for the design of practical IPT systems are given.

Table 1 Parameters of the Considered IPT System

Variable	Value	Variable	Value
L_1	75 µH	C_1	46.75 nF
L_2	75 µH	C_2	46.75 nF
k	0.25	$R_{L,eq}$	10 Ω
ω_0	2π·85 kHz	P_2	50 kW

2 Power at the Transformer Terminals

In order to simplify the calculations presented throughout the article, the first part of this section briefly reviews the fundamental frequency model of the series-series compensated IPT system. Afterwards, the instantaneous power at the terminals of the IPT coils and the energy flux across the air gap is calculated based on equivalent circuit diagrams.

2.1 Fundamental Frequency Model

Throughout the article, a series-series resonant compensation [17] is considered as shown in Fig. 1. The resonant capacitors are selected for a full compensation of the IPT coil self-inductances L_1 and L_2 according to

$$C_i = 1/(\omega_0^2 L_i), \tag{1}$$

where ω_0 represents the resonant frequency and $i \in [1, 2]$ stands for the transmitter and the receiver, respectively. This topology is often favored for the high partial load efficiency and for the coupling-independent resonant frequency. The position of the receiver coil with respect to the transmitter coil is variable in many practical applications. Therefore, a design which is robust with respect to variations of the magnetic coupling is generally preferable. However, the results presented herein are expected to apply similarly also for different resonant compensation topologies.

Because of the pronounced bandpass characteristics of the resonant circuit, the currents in the IPT system are approximately sinusoidal even though a full-bridge inverter producing a rectangular voltage waveform is typically used to drive the resonant circuit [cf. Fig. 1]. Therefore, the power is transferred almost exclusively by the voltage and current fundamental frequency components. Consequently, IPT systems are commonly described with the fundamental frequency equivalent circuit model given in Fig. 1. Throughout the article, the parameter values listed in Table 1 are used for the

calculations. Power losses are neglected ($R_{1,\mathrm{AC}} = R_{2,\mathrm{AC}} = 0$) until Section 4.2 at the very end of the article, where the transmission efficiency is calculated for an optimized design.

According to [16], the receiver-side rectifier with capacitive smoothing can be represented by the equivalent load resistance

$$R_{\mathrm{L,eq}} = \frac{8}{\pi^2}\frac{U_{2,\mathrm{DC}}^2}{P_2}, \tag{2}$$

where $U_{2,\mathrm{DC}}$ stands for the DC output voltage of the receiver-side rectifier stage and P_2 for the average output power.

The magnetic coupling k of the transmitter and the receiver coil is defined as

$$k = \frac{M}{\sqrt{L_1 L_2}}, \tag{3}$$

where M represents the mutual inductance of the coils. Therefore, from the equivalent circuit in Fig. 1, the relation between the phasors of the transmitter current $\underline{\hat{i}}_1$ and the receiver current $\underline{\hat{i}}_2$ follows as

$$\underline{\hat{i}}_2 = \mathrm{j}\frac{\omega_0 k\sqrt{L_1 L_2}}{R_{\mathrm{L,eq}}} \cdot \underline{\hat{i}}_1 \tag{4}$$

and the voltage transfer from the source $\underline{\hat{u}}_1$ to the load voltage $\underline{\hat{u}}_2$ follows

$$\underline{\hat{u}}_2 = \mathrm{j}\frac{R_{\mathrm{L,eq}}}{\omega_0 k\sqrt{L_1 L_2}} \cdot \underline{\hat{u}}_1 \tag{5}$$

It can be seen from (4)-(5), that as a result of the selected series-series compensation, the current and voltage phasors $\underline{\hat{i}}_1$ and $\underline{\hat{u}}_1$ at the source side and $\underline{\hat{i}}_2$ and $\underline{\hat{u}}_2$ at the load side are in phase. Therefore, only active power is supplied by the voltage source representing the transmitter-side full-bridge inverter. The reactive power required for magnetizing the IPT coils is supplied by the resonant capacitors, as is discussed later in the article.

Furthermore, (4) shows that the transmitter current $\underline{\hat{i}}_1$ and the receiver current $\underline{\hat{i}}_2$ are exactly 90° phase shifted, independently of the equivalent load resistance $R_{\mathrm{L,eq}}$ or the magnetic coupling k. From their time-domain waveforms, which are shown in Fig. 2(a), it can be seen that the magnetizing current $i_\mu = i_1 - i_2$ is of the same order of magnitude as i_1 and i_2 themselves. These are the key differences of an IPT system compared to a conventional transformer, where the magnetizing current is typically small and the primary and secondary currents are in phase.

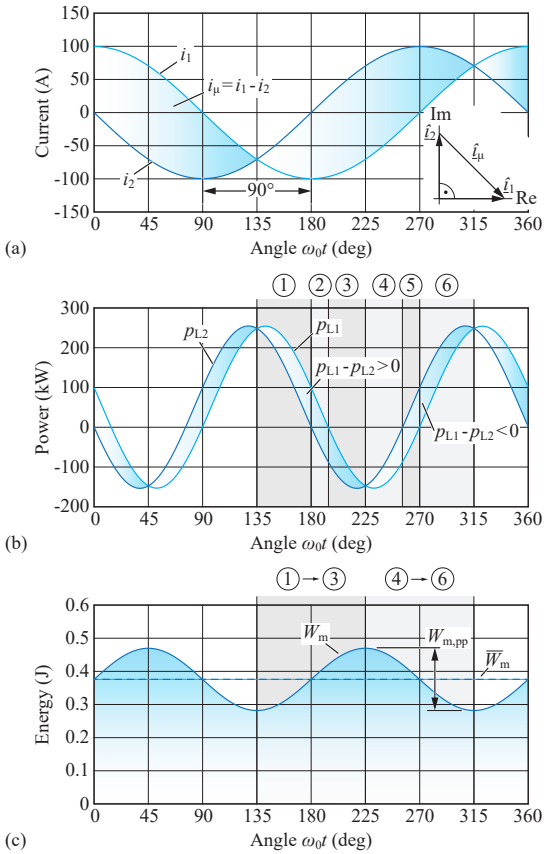

Fig. 2 (a) Waveforms and phasor diagram of the transmitter coil current i_1 and the receiver coil current i_2. (b) Instantaneous powers p_{L1} and p_{L2} at the terminals of the IPT coils. (c) Total magnetic energy W_m stored in the IPT coil inductances. All waveforms are calculated for an optimally designed IPT system with the values given in Table 1.

2.2 Terminal Power and Energy Transfer

For providing a more intuitive understanding of the energy exchange between the IPT coils and the time variation of the stored magnetic energy, the investigation is continued in the time domain even though the presented results could obtained analogously from a frequency domain analysis.

The instantaneous powers at the transformer input and output terminals are given by

$$p_{L1} = u_{L1} i_1 \quad \text{and} \quad p_{L2} = u_{L2} i_2, \tag{6}$$

respectively. The waveforms in Fig. 2(b) show that the power p_{L1} supplied to the IPT coils consists of an active part (average value of $p_{L1} \neq 0$), which according to the above observations is supplied by the source $\underline{\hat{u}}_1$, and a reactive part (p_{L1} is partly negative), which is supplied by the compensation capacitor C_1. The same applies analogously for the power p_{L2} at the transformer output terminals. The two components will be mathematically separated and discussed in detail in Section 4.1. At this point, the power transfer shall be investigated more closely directly with the waveforms.

Even though a lossless system is considered, the instantaneous powers at the input and output terminals of the IPT coils are not equal. In Fig. 2(b), the time intervals marked by ①-⑥ can be distinguished:

① $p_{L1} > p_{L2} > 0$: energy is supplied by the transmitter and extracted by the receiver. The difference $p_{L1} - p_{L2} > 0$ leads to inductive energy storage.
② $p_{L1} > 0 > p_{L2}$: energy is stored by the transmitter and the receiver coil.
③ $0 > p_{L1} > p_{L2}$: energy is supplied by the receiver and extracted by the transmitter. The difference $|p_{L2}| - |p_{L1}| > 0$ leads to energy storage.
④ $0 > p_{L2} > p_{L1}$: energy is supplied by the receiver and extracted by the transmitter. In addition, the transmitter extracts stored energy.
⑤ $p_{L2} > 0 > p_{L1}$: stored energy is extracted by the transmitter and the receiver coil.
⑥ $p_{L2} > p_{L1} > 0$: energy is supplied by the transmitter and extracted by the receiver. In addition, the receiver extracts stored energy.

Consequently, the magnetic energy W_m in the inductances of the IPT coils, which is given by

$$W_m = \frac{1}{2}\left(L_1 i_1^2 + L_2 i_2^2 - 2M i_1 i_2\right), \tag{7}$$

exhibits a time variation. As shown in Fig. 2(c), the magnetic energy increases during intervals ①-③ and decreases during ④-⑥. The resulting peak-to-peak energy oscillation $W_{m,pp}$ is a result of the periodic magnetization and demagnetization, which causes the reactive power demand of the IPT coils.

3 Electromagnetic Fields and Poynting Vector

So far, only the transformer terminal characteristics were analyzed. However, an intuitive understanding of the periodic energy storage and extraction process that causes the contactless energy transfer can only be obtained from a closer look at the electromagnetic fields. Therefore, in this section, the energy exchange between the transmitter and receiver coils is investigated using Finite Element Method (FEM) simulations and Poynting's theorem.

3.1 Considered 2D-FEM Model

A two dimensional (2D) model with axial symmetry as shown in Fig. 3(a) is considered. At the model borders, the magnetic field is specified to have only a tangential vector component. Furthermore, a constant current density is imposed for the conductors (without induced currents), which corresponds to the model of a perfect litz wire. The material of the surroundings is air.

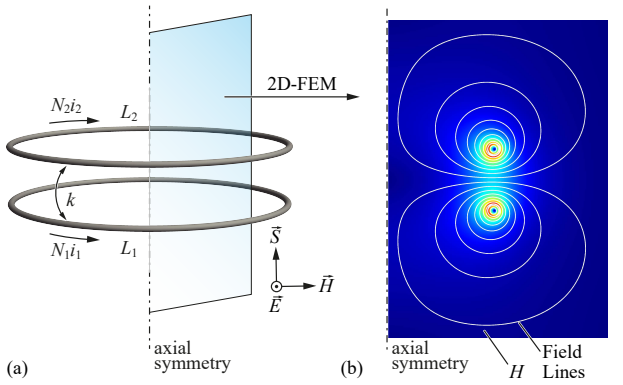

Fig. 3 (a) Schematic drawing of the three dimensional, axis symmetric IPT coil arrangement. (b) 2D-FEM simulation result for the magnitude of the magnetic field H at time $\omega_0 t = 135°$.

The considered simplified FEM model is sufficient for the educational purpose pursued in this article, because the all significant effects are captured and no additional insight could be obtained from a more complex IPT coil structure. For consistency with the previous sections, time domain simulations are used. Because of the simplified 2D-FEM model, the computation time is already low and it is not necessary to change to the frequency domain, as is usually preferred for the FEM analysis of more complex IPT coil designs.

For calibrating the 2D-FEM model, the diameter of the IPT coils is adjusted such that the magnetic coupling k matches the value given in Table 1 for a fixed air gap of 100 mm and a wire diameter of 20 mm. This results in an IPT coil diameter of 400 mm (measured between the conductor centers). Similarly, the turns numbers are adjusted until the self-inductance L_1 and L_2 obtained from the FEM simulation match the values given in the table, which leads to $N_1 = N_2 = 9.6$ (turns numbers $N_i \notin \mathbb{N}$ are used for making the simulation more accurate).

The 2D-FEM calculation result for the magnitude of the magnetic field H at $\omega_0 t = 135°$ is shown in Fig. 3(b) together with contour lines of the magnetic vector potential (field lines). It is interesting to note that even though the magnetic coupling is $k = 0.25$ there are no field lines crossing both coils, because for $i_1 = i_2$ the fields cancel exactly at this point in time [cf. Fig. 2(a)].

3.2 Analysis of Energy Flux

The contactless energy transfer through the air surrounding the IPT coils is described by the Poynting vector (or energy flux density)

$$\mathbf{S} = \mathbf{E} \times \mathbf{H}, \tag{8}$$

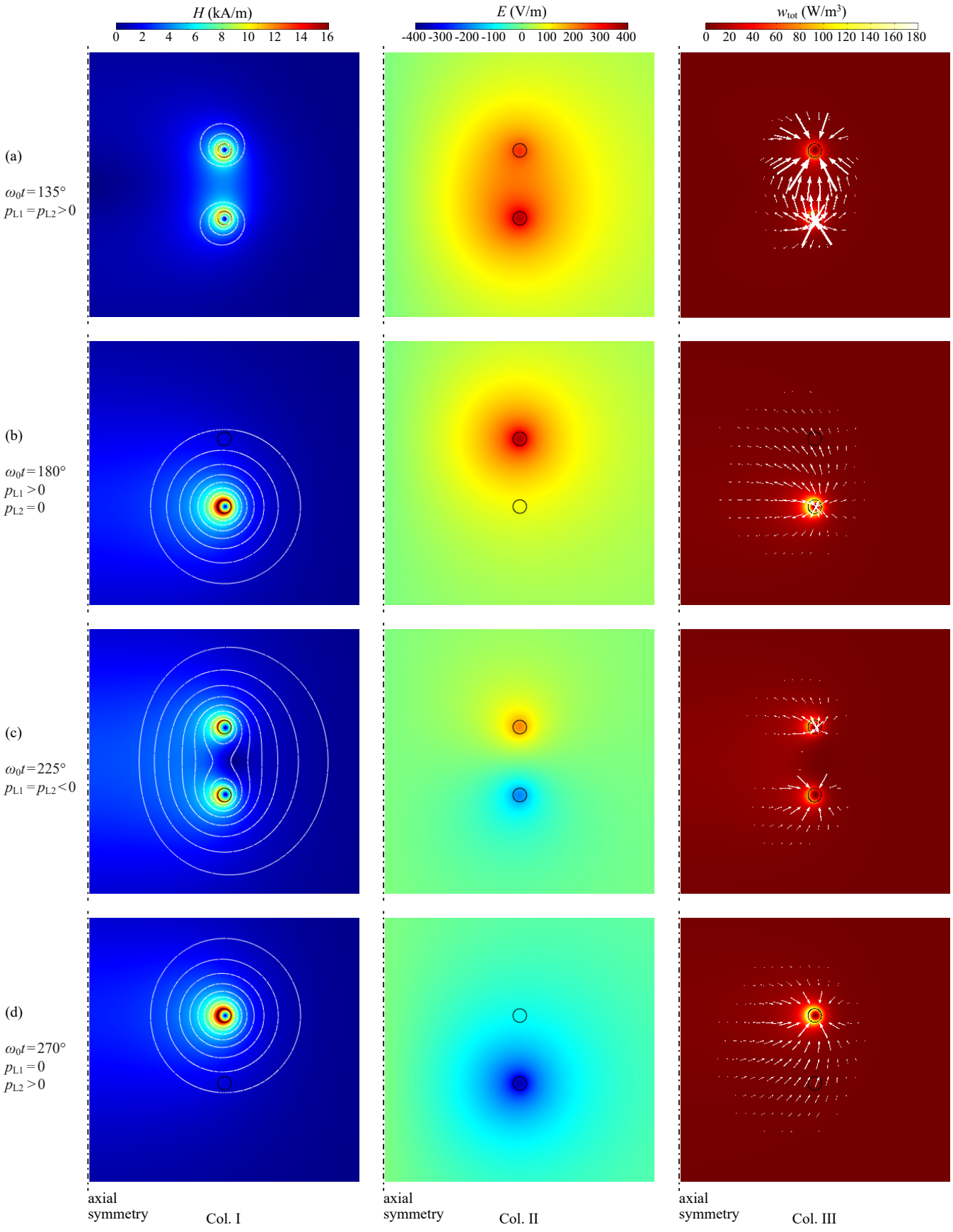

Fig. 4 Time sequence of FEM calculation results for the 2D axis-symmetric model of Fig. 3. The plots in column I show the magnitude of the magnetic field **H** and contour lines of the magnetic vector potential **A** (field lines). The plots in column II shows the magnitude of the electric field $\mathbf{E} = -\partial\mathbf{A}/\partial t$. The plots in column III show the total energy density w_{tot} and an arrow plot of the Poynting vector $\mathbf{S} = \mathbf{E} \times \mathbf{H}$.

where the magnitude of **S** represents the local change in energy per unit time and unit area. The orientation of **S** is the direction of the energy flux [8,12,13]. In the considered axis-symmetric coil arrangement, the **E**, **H**, and **S** vector fields form a right-handed system as indicated in Fig. 3(a).

The electric field **E** is generally given by

$$\mathbf{E} = -\nabla\phi - \frac{\partial \mathbf{A}}{\partial t}, \tag{9}$$

where ϕ is the electric potential and **A** is the magnetic vector potential (which in the considered 2D case has only a vector component pointing out of the plane and could therefore be simplified to a scalar). However, for the following discussion, the capacitive component $-\nabla\phi$ is neglected, because it does not contribute to the contactless power transfer.

Due to the presence of the electric field, there is also an electric energy component that needs to be included in addition to the magnetic energy of (7). The total energy density is given as

$$w_{\mathrm{tot}} = w_{\mathrm{m}} + w_{\mathrm{e}} = \frac{1}{2}\mu_0 H^2 + \frac{1}{2}\varepsilon_0 E^2 \tag{10}$$

and the total energy of the system follows by integration over the volume of the simulated domain Ω

$$W_{\mathrm{tot}} = \iiint_{\Omega} w_{\mathrm{tot}}\, \mathrm{d}\Omega \tag{11}$$

The considerations of the previous section are nevertheless accurate as the electric energy density w_{e} is small compared to the magnetic energy component w_{m} in the investigated frequency range (tens of kHz). Only for high frequencies, the induced electric field $-\partial\mathbf{A}/\partial t$ is large enough for the electric energy density to become significant.

According to the definition of the Poynting vector [8, 12, 13], the divergence of **S** must be equal to the local change of the total energy density

$$\boldsymbol{\nabla} \cdot \mathbf{S} = -\frac{\partial w_{\mathrm{tot}}}{\partial t}, \tag{12}$$

where no materials with ohmic losses, polarization losses, or magnetization losses are considered. Therefore, the energy transfer from the transmitter to the receiver can be calculated by integrating the Poynting vector over the surfaces A_1 and A_2 of the transmitter and the receiver coil, respectively. The power leaving the transmitter coil is given by

$$p_{\mathrm{L1}} = \oiint_{A_1} \mathbf{S} \cdot \mathrm{d}\mathbf{A}_1 \tag{13}$$

and the power entering the receiver coil follows from

$$p_{\mathrm{L2}} = -\oiint_{A_2} \mathbf{S} \cdot \mathrm{d}\mathbf{A}_2, \tag{14}$$

where the unit vectors $\mathrm{d}\mathbf{A}_1$ and $\mathrm{d}\mathbf{A}_2$ are oriented out of the respective conductor.

As discussed in Section 2.2, the power p_{L1} that is supplied to the IPT coils and the power p_{L2} leaving the system at the receiver are not equal. Their difference

$$p_{\mathrm{L1}} - p_{\mathrm{L2}} = \frac{\partial W_{\mathrm{tot}}}{\partial t} \tag{15}$$

represents the reactive power that is used to periodically magnetize (or *energize*) and demagnetize (or *deenergize*) the IPT coils.

The periodic energy storage and extraction processes discussed in Section 2.2 can also be observed in the field patterns obtained from the FEM simulation. A time sequence of FEM results for the magnetic field, the electric field, and the Poynting vector is shown in Fig. 4. In column I, the magnitude of the magnetic field H is shown together with contour lines of the magnetic vector potential **A** (field lines). Column II shows the magnitude of the electric field E. In column III, the total energy density w_{tot} is shown together with an arrow plot of the Poynting vector **S**.

Fig. 4(a) shows the fields at time $\omega_0 t = 135°$, which was already shown above. This instant marks the beginning of interval ①, when the input power p_{L1} and the output power p_{L2} of the IPT coils are equal and positive [cf. Fig. 2(b)]. As mentioned previously, there are no field lines crossing both IPT coils, because the fields cancel exactly. Nevertheless, power is transferred from the transmitter to the receiver, as confirmed by the Poynting vector in column III. At the time instant shown in Fig. 4(b), the power p_{L2} at the receiver terminals reaches zero, which marks the transition from interval ① to interval ②. Then, the transmitter stores energy in the electric and magnetic fields, which is confirmed by the Poynting vector field showing an energy flux that vanishes in the air surrounding the coils, i. e., **S** has non-zero divergence in the air, confirming (12). The time instant of Fig. 4(c) marks the transition between interval ③ and interval ④, when p_{L1} and p_{L2} are equal and negative. At this instant, the receiver supplies energy, while the transmitter extracts energy that was previously stored in the electric and magnetic fields as confirmed by the Poynting vector. In Fig. 4(d), the power at the transmitter reaches zero while the power at the receiver is already positive. This marks the transition between interval ⑤ and interval ⑥. At the shown time instant, the receiver extracts previously stored energy from the electric and magnetic fields.

The observed periodic process of electromagnetic energy storage and extraction is inherently required for the contactless energy transfer (otherwise, the induced electric field

$-\partial\mathbf{A}/\partial t$ and therefore also the Poynting vector vanishes). However, the amount of reactive power that is required for the interaction with the fields varies with the design of the resonant circuit. It is intuitively clear that a minimization of the reactive power leads to a design with the lowest IPT coil currents i_1 and i_2, and therefore ultimately to the highest transmission efficiency. This approach is pursued in the next section, where guidelines for an efficiency optimal design of the IPT system are derived.

4 Optimal IPT System Design

In this section, a minimization of the reactive power demand of the IPT coils is performed. The analysis reveals the conditions for an efficiency optimal design of the IPT system. The obtained guidelines coincide with the design rules that are commonly used in the relevant literature, as confirmed at the end of the section.

4.1 Reactive Power Demand of Contactless Transformer

Using the time-domain equivalent of (4), the instantaneous input power p_{L1} of the IPT coils it can be expressed as

$$p_{\mathrm{L1}} = P_2 + P_2\cos(2\omega_0 t) - \underbrace{\frac{P_2}{k}\frac{R_{\mathrm{L,eq}}}{k\omega_0 L_2}\sin(2\omega_0 t)}_{=:q_{\mathrm{L1}}} \tag{16}$$

Similarly, the output power p_{L2} is given by

$$p_{\mathrm{L2}} = P_2 - P_2\cos(2\omega_0 t) - \underbrace{\frac{P_2}{k}\frac{k\omega_0 L_2}{R_{\mathrm{L,eq}}}\sin(2\omega_0 t)}_{=:q_{\mathrm{L2}}} \tag{17}$$

The instantaneous powers p_{L1} and p_{L2} consist of an active power component, given by $P_2 \pm P_2\cos(2\omega_0 t)$. This power component is supplied by the voltage source $\underline{\hat{u}}_1$ and dissipated in the load resistance $R_{\mathrm{L,eq}}$. The observed oscillation of the instantaneous active power with $2\omega_0$ is characteristic for single-phase AC systems and cannot be avoided. In addition to the active power, the instantaneous powers contain the reactive power components q_{L1} and q_{L2}, which are necessary for magnetizing the transformer. They are supplied by the resonant compensation capacitors C_1 and C_2, respectively.

As shown by (15), the energy supplied to the electric and magnetic fields is given by

$$\frac{\partial W_{\mathrm{tot}}}{\partial t} = p_{\mathrm{L1}} - p_{\mathrm{L2}} = 2P_2\cos(2\omega_0 t)\ldots + \ldots + \frac{P_2}{k}\left(\frac{k\omega_0 L_2}{R_{\mathrm{L,eq}}} - \frac{R_{\mathrm{L,eq}}}{k\omega_0 L_2}\right)\sin(2\omega_0 t) \tag{18}$$

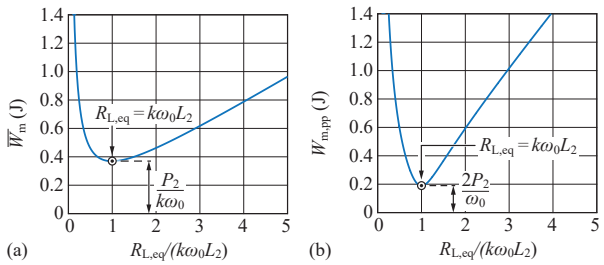

Fig. 5 (a) Average value $\overline{W}_{\mathrm{m}}$ and (b) peak-to-peak oscillation $W_{\mathrm{m,pp}}$ of the magnetic energy W_{m} as a function of the load factor $R_{\mathrm{L,eq}}/(k\omega_0 L_2)$.

if the electric energy is neglected. The reactive power demand is therefore minimized by adjusting the impedances $\omega_0 L_2$ and $R_{\mathrm{L,eq}}$ to fulfill the condition

$$R_{\mathrm{L,eq}} = k\omega_0 L_2 \tag{19}$$

As shown in Fig. 5, for this condition the average value of the magnetic energy $\overline{W}_{\mathrm{m}}$ and the peak-to-peak oscillation $W_{\mathrm{m,pp}}$ [cf. Fig. 2(c)] are minimized simultaneously. The remaining reactive power, which is given by

$$q_{\mathrm{L1}} = q_{\mathrm{L2}} = \frac{P_2}{k}\sin(2\omega_0 t), \tag{20}$$

constitutes the minimum requirement of the IPT coils for the transfer of the output power P_2 across the air. Therefore, this condition leads to the smallest possible IPT coil currents.

4.2 IPT System Design Guidelines

The design of an IPT system starts with the specification of the desired output power P_2 and DC output voltage $U_{2,\mathrm{DC}}$, from which in a fist design step the equivalent load resistance $R_{\mathrm{L,eq}}$ is calculated using (2). For the design of the IPT coil self-inductances, the design guidelines for minimum IPT coil currents follow from (19) and (5) as

$$L_2 = \frac{R_{\mathrm{L,eq}}}{k\omega_0} \quad \text{and} \quad L_1 = L_2 \cdot \left(\frac{U_{1,\mathrm{DC}}}{U_{2,\mathrm{DC}}}\right)^2 \tag{21}$$

for a series-series compensated IPT system operated at the resonant frequency ω_0. Condition (19) has been rearranged, because the designer can adjust the IPT coil self-inductances L_1 and L_2 in an iterative process based on FEM simulations by modifying the turns numbers, but he cannot influence the magnetic coupling k, which is mainly given by the geometric properties of the coil arrangement. The equivalent load resistance $R_{\mathrm{L,eq}}$, which is given by the output voltage and the output power, can only be influenced by the designer if an impedance transformation with either a transformer or a dedicated power electronic converter is implemented as

in [2, 7]. The frequency ω_0 constitutes another design parameter, but it is typically fixed either by a standard or the design considerations for the power electronics.

For IPT system designs that fulfill (21), the relation between the transmitter current $\underline{\hat{i}}_1$ and the receiver current $\underline{\hat{i}}_2$ at the resonant frequency ω_0 is given by

$$\underline{\hat{i}}_2 = \mathrm{j} \cdot \sqrt{\frac{L_1}{L_2}} \cdot \underline{\hat{i}}_1 \tag{22}$$

For the input voltage to and output voltage transfer function, the result is

$$\underline{\hat{u}}_2 = \mathrm{j} \cdot \sqrt{\frac{L_2}{L_1}} \cdot \underline{\hat{u}}_1 \tag{23}$$

If AC losses in the IPT coil windings are considered ($R_{1,\mathrm{AC}}$, $R_{2,\mathrm{AC}} > 0$ in Fig. 1), the efficiency of the power transfer from the source $\underline{\hat{u}}_1$ to the load $R_{\mathrm{L,eq}}$ results as

$$\eta = \frac{(kQ)^2}{\left(1 + \sqrt{1 + (kQ)^2}\right)^2}, \tag{24}$$

where $Q = \sqrt{Q_1 Q_2}$ has been introduced for the geometric mean of the quality factors Q_1 and Q_2 of the transmitter and the receiver coil, respectively, which are given by $Q_i = \omega_0 L_i / R_{\mathrm{AC},i}$ and $i \in [1, 2]$.

This result demonstrates that the guideline (19) leads to the maximum attainable efficiency of the IPT system as calculated, e. g., in [2, 14, 15, 17]. It is therefore the condition for an efficiency optimal design of the series-series compensated IPT coils. Additionally, the minimization of the reactive power also implies the smallest energy storage capability for the resonant capacitors, which results in the smallest volume and lowest capacitor losses.

It should be noted that as shown in [3, 15], the same maximum efficiency can also be reached with a series-parallel compensation, with conditions for $\omega_0 L_2$ and $R_{\mathrm{L,eq}}$ that only slightly differ from (19). Therefore, it is expected that an analogous derivation could be made also for other resonant compensation topologies, even though in this paper only a series-series resonant compensation is analyzed.

5 Conclusion

In this article, the contactless energy transfer of an IPT system was analyzed with the help of the terminal characteristics of the contactless transformer as well as based on electromagnetic field theory. It was shown that the contactless energy transfer across the air gap results from the interaction of the electric circuits with the electromagnetic fields by a periodic charging and discharging process. Furthermore, a minimization of the reactive power demand of the contactless transformer was performed. The result coincides with the known conditions for an efficiency optimal design of series-series compensated IPT systems. The obtained design guidelines can be directly applied for an optimized design of contactless power supplies for various applications.

References

1. Bocan, K., Sejdić, E.: Adaptive transcutaneous power transfer to implantable devices: A state of the art review. Sensors **16**(3), 393 (2016). DOI 10.3390/s16030393
2. Bosshard, R.: Multi-objective optimization of inductive power transfer systems for EV charging. Ph.D. thesis, ETH Zurich, Switzerland (2015)
3. Bosshard, R., Kolar, J.W., Mühlethaler, J., Stevanović, I., Wunsch, B., Canales, F.: Modeling and η-α-Pareto optimization of inductive power transfer coils for electric vehicles. IEEE J. Emerg. Select. Topics Power Electron. **3**(1), 50–64 (2015). DOI 10.1109/JESTPE.2014.2311302
4. Brandão Faria, J.A.: Poynting vector flow analysis for contactless energy transfer in magnetic systems. IEEE Trans. Power Electron. **27**(10), 4292–4300 (2012). DOI 10.1109/TPEL.2012.2191421
5. Choi, S., Gu, B., Jeong, S., Rim, C.: Advances in wireless power transfer systems for roadway-powered electric vehicles. IEEE J. Emerg. Select. Topics Power Electron. **3**(1), 18–36 (2015). DOI 10.1109/JESTPE.2014.2343674
6. Covic, G., Boys, J.: Inductive power transfer. Proc. IEEE **101**(6), 1276–1289 (2013). DOI 10.1109/JPROC.2013.2244536
7. Diekhans, T., De Doncker, R.: A dual-side controlled inductive power transfer system optimized for large coupling factor variations and partial load. IEEE Trans. Power Electron. **30**(11), 6320–6328 (2015). DOI 10.1109/TPEL.2015.2393912
8. Ferreira, J.A.: Application of the Poynting vector for power conditioning and conversion. IEEE Trans. Educ. **31**(4), 257–264 (1988). DOI 10.1109/13.9751
9. Goeldi, B., Reichert, S., Tritschler, J.: Design and dimensioning of a highly efficient 22 kW bidirectional inductive charger for e-mobility. In: Proc. Int. Exhibition and Conf. for Power Electronics (PCIM Europe), pp. 1496–1503. Nuremberg, DE (2013)
10. Hui, S.Y.: Planar wireless charging technology for portable electronic products and Qi. Proc. IEEE **101**(6), 1290–1301 (2013). DOI 10.1109/JPROC.2013.2246531
11. Hui, S.Y., Zhong, W.X., Lee, C.K.: A critical review of recent progress in mid-range wireless power transfer. IEEE Trans. Power Electron. **29**(9), 4500–4511 (2014). DOI 10.1109/TPEL.2013.2249670
12. Jackson, J.D.: Classical Electrodynamics, 3 edn. John Wiley & Sons, Inc., Hoboken, USA (1998)
13. Leuchtmann, P.: Einführung in die elektromagnetische Feldtheorie, 1 edn. Pearson Studium, Munich, DE (2005)
14. Schuder, J.C.: Powering an artificial heart: birth of the inductively coupled-radio frequency system in 1960. Artificial Organs **26**(11), 909–915 (2002)
15. van Schuylenbergh, K., Puers, R.: Inductive Powering: Basic Theory and Application to Biomedical Systems, 1 edn. Springer Science+Business Media, Dordrecht, NL (2009). DOI 10.1007/978-90-481-2412-1
16. Steigerwald, R.: A comparison of half-bridge resonant converter topologies. IEEE Trans. Power Electron. **3**(2), 174–182 (1988). DOI 10.1109/63.4347

17. Waffenschmidt, E., Staring, T.: Limitation of inductive power transfer for consumer applications. In: Proc. 13th European Conf. on Power Electronics and Applications (EPE - ECCE Europe), pp. 1–10. Barcelona, ES (2009)